Eur Phys J A (2004) **19**, s01, 213–221
Digital Object Identifier (DOI) 10.1140/epjad/s2004-03-036-6

EPJ A direct
electronic only

The study of high density matter at RHIC

Survey of experimental results from RHIC

Thomas S. Ullrich

Brookhaven National Laboratory, Upton New York 11973-5000, USA

Received: 30 Jul / Accepted: 14 Nov 2003 /
Published Online: 6 Feb 2004 – © Società Italiana di Fisica / Springer-Verlag 2004

Abstract. QCD predicts a phase transition between hadronic matter and a Quark Gluon Plasma at high energy density. The Relativistic Heavy Ion Collider (RHIC) at Brookhaven National Laboratory is a new facility dedicated to the experimental study of matter under extreme conditions. Already the first round of experimental results at RHIC indicated that the conditions to create a new state of matter are indeed reached in the collisions of heavy nuclei. Studies of particle spectra and their correlations at low transverse momenta provide evidence of strong pressure gradients in the highly interacting dense medium and hint that we observe a system in thermal equilibrium. Recent runs with high statistics allow us to explore the regime of hard-scattering processes where the suppression of hadrons at large transverse momentum, and quenching of di-jets are observed thus providing further evidence for extreme high density matter created in collisions at RHIC.

PACS. 25.75.-q Relativistic heavy-ion collisions

1 Introduction

At high temperature, hadronic matter dissolves into a soup of its constituent quarks and gluons. For an asymptotically free field theory such as QCD, the state of matter at high energy density is simple: long range (low momentum) interactions are screened, and short range (high momentum) interactions are weak, leading to an ideal gas equation of state in the high energy density limit [1]. At temperature $T \gg \Lambda_{\rm QCD}$ matter is a gas of deconfined, weakly interacting quarks and gluons (the "Quark-Gluon Plasma", or QGP), whereas at $T \ll \Lambda_{\rm QCD}$ quarks and gluons are confined and matter consists of strongly interacting hadrons.

The QCD phase diagram has a complex structure [2]. At low temperature and low baryon density the phase is hadronic (confined phase) and chiral symmetry is broken. Color-superconducting and other phases may exist at high baryon density and low temperature [3], whereas at high temperature the quarks and gluons are deconfined and chiral symmetry is restored. The early universe descended from high T at extremely small μ_B. Neutron star cores have high μ_B and very low T.

First-principles calculations of finite temperature QCD can only be carried out numerically on the lattice [4]. These calculation show that the energy density ϵ exhibits a sharp rise in the vicinity of the critical temperature T_C, indicating a rapid change in the number of underlying degrees of freedom. However, the ideal gas Stefan-Boltzmann limit $\epsilon_{\rm SB}$ has not yet been achieved at $T \sim 4T_C$. Putting in physical values, $T_C \sim 175$ MeV, resulting in critical energy density $\epsilon_C = (6 \pm 2) T_C^4 \sim 0.7$ GeV/fm^3. This value should be kept in mind for comparison to conditions achieved in laboratory experiments.

The order of the deconfinement phase transition can be determined in some limiting cases [4]. It is first order for pure gauge and for three light quarks, second order for two light and one heavy quark. For physical quark masses the order of the transition, or indeed whether it is a smooth cross over, has not been determined. The extension of lattice calculations to $\mu_B > 0$ is a long-standing problem, but there has been significant recent progress in determining the phase boundary and equation of state for finite μ_B [6].

In the early universe, the confinement transition (QGP $\rightarrow$ hadrons) at very low μ_B occurred about 10 μs after the big bang [7]. A strongly first order phase transition may have generated primordial black holes, strange quark nuggets, or local baryon asymmetries affecting primordial nucleosynthesis, though no relics of this transition have been observed thus far. In the cores of neutron stars, a QGP phase at low temperature and high μ_B may generate observable millisecond pulsar phenomena [8].

It is natural to ask whether the deconfinement and chiral symmetry restoration transitions can be studied in accelerator-based experiments. We require a system having temperature of order the pion mass in equilibrium over a large volume. The best possibility to accomplish this is

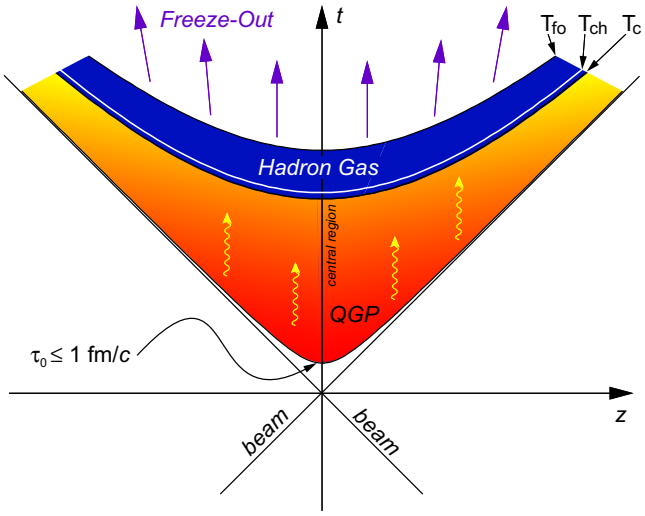

Fig. 1. The space-time picture of relativistic heavy-ion collisions, proceeding through the following stages: formation, deconfined state (QGP), hadron gas (T_C), chemical freezeout ($T_{\rm ch}$), thermal freezeout ($T_{\rm fo}$), and free streaming

through the collision of heavy nuclei at the highest possible energy.

However, nuclear collisions at high energy are highly dynamic. Even if a hot, equilibrated system is created early in the collision, it will immediately expand and cool. If a QGP is formed it will hadronize after a brief period, and signatures from the deconfined phase may be masked by those from the hot, interacting hadron gas. The central issue is to find and measure those experimental observables that are sensitive to the state of matter early in the collision [9].

Broadly speaking, several epochs in the evolution of high energy nuclear collisions can be sketched as depicted in Fig. 1. Immediately following the collision is a brief formation time $\tau < 1{\rm fm}/c$, during which large momentum transfer (short-distance) processes occur. It is also during this period that the highest energy density is achieved and the QGP may result. After an expansion time of perhaps a few fm/c the plasma hadronizes into a dense, interacting hadron gas. Further expansion and cooling causes the temperature to fall to the point at which inelastic collisions among hadrons cease (*chemical freezeout*) and the relative populations of the various long-lived hadron species are established. Elastic collisions continue until *kinetic freezeout*, after which point the hadrons fly effectively undisturbed to the detectors. Thus, the relative populations of stable hadrons reflect the conditions at chemical freezeout, whereas their momentum spectra reflect the conditions at kinetic freezeout. More penetrating probes (dileptons, direct photons, jets, heavy quarks,...) may carry information on the conditions around the time of their formation earlier in the collision.

Collisions of heavy nuclei at ultra-relativistic energies have been studied in fixed target experiments at the Brookhaven AGS and CERN/SPS for the past 15 years. In 1999, the Relativistic Heavy Ion Collider (RHIC) at Brookhaven National Laboratory was commissioned, bringing into operation the first facility largely dedicated to the study of matter at high energy density.

I will first describe the RHIC machine and experiments and then discuss some of the main results from its heavy ion physics program. I will briefly touch on "soft physics" observables ($p_T \lesssim 2$ GeV/c) and summarize what has been learned from them. The second part of the review concentrates on the major new development at RHIC: jet production and indications of partonic interactions with dense matter, which may directly probe the energy density achieved early in the collision.

2 The relativistic heavy ion collider and experiments

RHIC consists of two concentric superconducting rings, 3.8 km in length. It has enormous flexibility in beam masses and energies, with capability to collide gold ions from $\sqrt{s_{\rm NN}} = 20$ to 200 GeV per nucleon pair, protons up to $\sqrt{s} = 500$ GeV, and asymmetric systems, most importantly protons and deuterons with heavy nuclei. The top center-of-mass energy for heavy nuclei is a factor of 10 larger than for the fixed target experiments at the CERN/SPS, extending significantly the statistical and transverse momentum reach of many observables and opening up new channels. RHIC is also the first polarized proton collider, creating new opportunities to study the spin content of the proton, in particular the contribution of the gluon at low $x_{\rm Bj}$. More details of the machine and its first year performance can be found in [10].

Design luminosity for Au+Au at 200 GeV is $\mathcal{L} = 2 \cdot 10^{26}$ cm^{-2}sec^{-1}, giving an interaction rate of about 2 kHz. While this luminosity appears to be tiny relative to other modern colliders, recall that the rate for hard processes such as jet production in nuclear collisions scales as $\sim A^2$ (A=atomic mass), so that hard process rates in Au+Au at design luminosity are the same as at a proton collider with $\mathcal{L} \approx 10^{31}$ cm^{-2}sec^{-1}. The design luminosity for p+p collisions at 500 GeV is $2 \cdot 10^{32}$ cm^{-2}sec^{-1}, with an interaction rate of about 8 MHz. Design polarization for p+p is 70%.

RHIC has six intersection regions, of which four are currently instrumented with experiments [11] (see Fig. 2). PHENIX consists of an axial field magnet and four independent spectrometers: two at midrapidity containing tracking, ring imaging Cerenkov counters, time of flight, and electromagnetic calorimetry, which are optimized for precision lepton, photon and hadron measurements, and two forward muon arms. STAR has conventional collider detector geometry, with a large solenoidal magnet, Time Projection Chamber for tracking, large coverage EM calorimetry, and an inner silicon-based tracker. STAR is designed for hadron, jet, lepton and photon measurements over large acceptance, as well as studies of event-wise fluctuations in high multiplicity nuclear collisions. BRAHMS consists of two small acceptance spectrometers for inclusive identified hadron measurements over wide

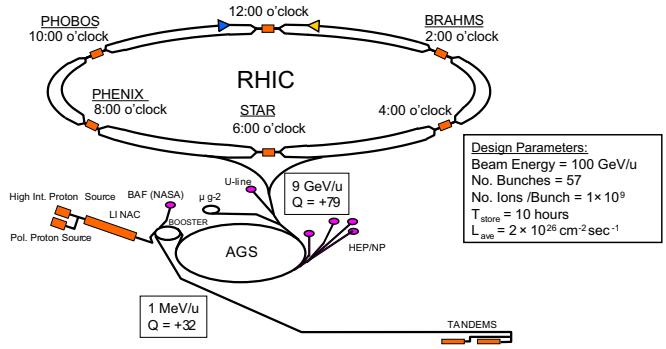

Fig. 2. The Relativistic Heavy Ion Collider (RHIC) accelerator complex at Brookhaven National Laboratory

phase space. PHOBOS has very wide phase space coverage for charged particles using silicon detectors, and a mid-rapidity spectrometer based on a dipole magnet, silicon tracking and Time of Flight. STAR and PHENIX each have about 450 collaborators, whereas PHOBOS and BRAHMS each have fewer than 100.

RHIC had a brief commissioning run in 1999. The data reported here are from a Au+Au run at $\sqrt{s_{\rm NN}}$ =130 GeV in 2000 and Au+Au and polarized p+p (∼15% polarization) runs at $\sqrt{s_{\rm NN}}$ = 200 GeV in 2001-2. The integrated luminosity is about 80 μb^{-1} for Au+Au and 1 pb^{-1} for p+p. A comprehensive view of the physics program of RHIC and what has been achieved thus far can be found in the proceedings of the recent Quark Matter conferences [12,13].

Nuclei are extended objects, and high energy nuclear collisions can be characterized experimentally as head-on ("central") or glancing ("peripheral"). The RHIC experiments all have different methods of determining the geometry, or centrality, of the collisions. In general, all measure some final state variable (or combination of these variables) that can be related to fractions of the total measured hadronic cross-section. Typical final state variables are the charged particle multiplicity at central or forward rapidities and the forward-going "spectator" neutrons that are measured in zero-degree calorimeters situated downstream of the interaction region. These centrality bins are then mapped to variables that allow for direct comparison between experiments. The primary variables that are used for comparison are *(i)* the number of participating nucleons in the collision $N_{\rm part}$ and *(ii)* the number of independent binary N+N collisions $N_{\rm bin}$, which are determined via the application of the Glauber model phenomenology. The basic concept of the Glauber model is to treat a Au+Au collision as a superposition of many independent nucleon-nucleon (N+N) collisions. Thus, the only parameters that the model depends on are the nuclear density profile (Woods-Saxon) and the non-diffractive inelastic N+N cross-section. The former is well measured in e+Au scattering experiments and the latter is well established by many previous experiments. With this, $N_{\rm bin}$ and $N_{\rm part}$ can be calculated as a function of impact parameter. Once the distributions $d\sigma/dN_{\rm part}$ and $d\sigma/dN_{\rm bin}$ are determined, these histograms are binned according to fractions of the total cross-section. This then determines the mean values of $N_{\rm bin}$ and $N_{\rm part}$ for each centrality class.

Phenomenologically it has been found that total particle production scales roughly as $N_{\rm part}$, whereas the rate of hard processes will scale as $N_{\rm bin}$ in the absence of nuclear effects. Such scaling rules can be used to uncover the new physics present in nuclear collisions. For instance, the violation of $N_{\rm bin}$ scaling at high-p_T indicates significant effects of the nuclear medium on high-p_T processes.

3 General characteristics of RHIC collisions

3.1 Global observables

One of the earliest probes suggested for QGP formation involves a study of the global parameters of the events, e.g. the energy deposition, multiplicity, and the average transverse momentum of the emitted particles, as a function of center-of-mass energy $\sqrt{s_{\rm NN}}$, mass number A, and centrality of the collision. For example, by studying the multiplicity of the produced particles one might estimate theoretically the entropy produced in the collision. Sudden changes in behavior with varying centrality or A would be indicators of a phase transition. So far, however, no such anomalous changes have been observed, at either the AGS, SPS, or RHIC. All results on global observables so far indicate a rather smooth evolution in centrality and $\sqrt{s_{\rm NN}}$. This, of course, does not necessarily imply the absence of a phase transition, but might be rather an indication of either the insensitivity of these observables to the early phase of the collision and/or might suggest a second order phase transition (or a cross-over). With the commencement of the RHIC program the question of multiparticle production in nuclear collisions became more complex due to the poorly understood role of perturbative QCD (hard processes).

Figure 3 from the PHOBOS Collaboration [14] shows charged particle multiplicity distributions $dN_{ch}/d\eta$ vs η over the full RHIC phase space, for Au+Au collisions at all three collision energies studied so far. The longitudinal phase space growth with increasing energy is apparent, as well as the increase in multiplicity for more central collisions. For the most central collisions at $\sqrt{s_{\rm NN}}$ = 130 GeV, 4200 charged particles are produced in the full phase space.

The distributions exhibit a central plateau near $\eta \sim 0$, indicating that the system has approximate longitudinal boost invariance. More detailed considerations of identified particle spectra show that boost invariance holds over a rather smaller region $\Delta y \sim 1$ [15].

The interpretation of the scaling of the multiplicity at mid-rapidity as a function of $N_{\rm part}$ appears still ambiguous. A simple model by Kharzeev and Nardi (KN) explains the dependence in a two-component approach differentiating between soft processes scaling with $N_{\rm part}$ and hard processes scaling with $N_{\rm bin}$ [16]. When fit to the data as shown in Fig. 4 by the PHOBOS collaboration the model allows one to extract the fraction of particles

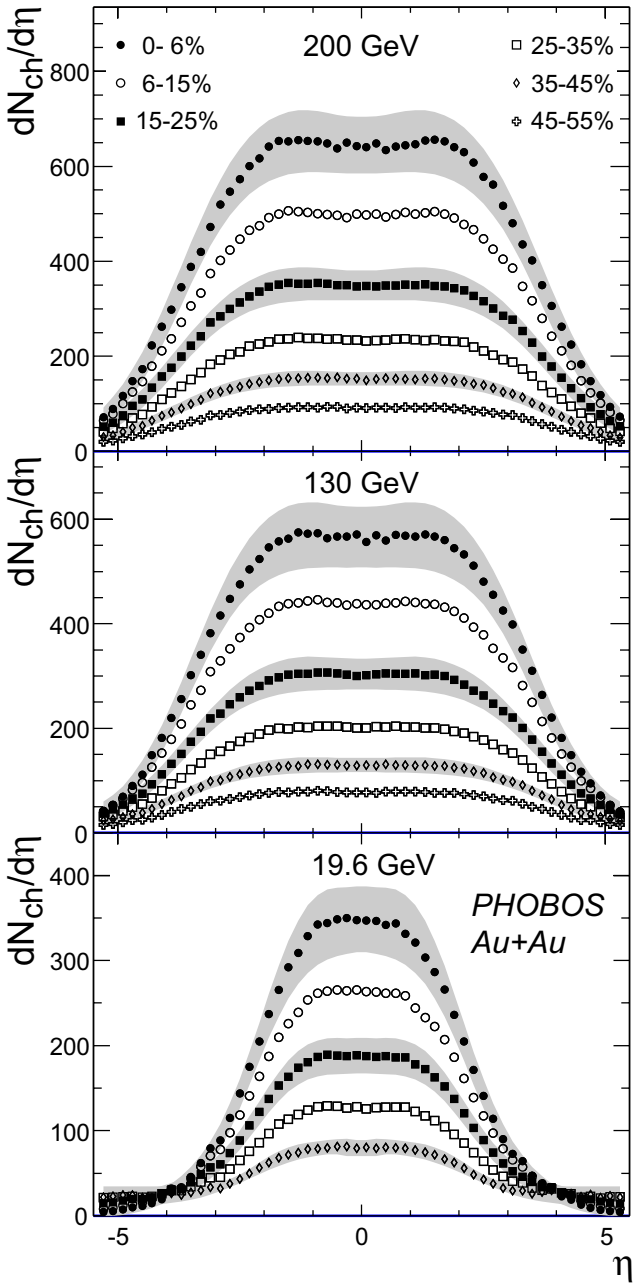

Fig. 3. $dN_{ch}/d\eta$ for various collision centralities over the full RHIC phase space [14]

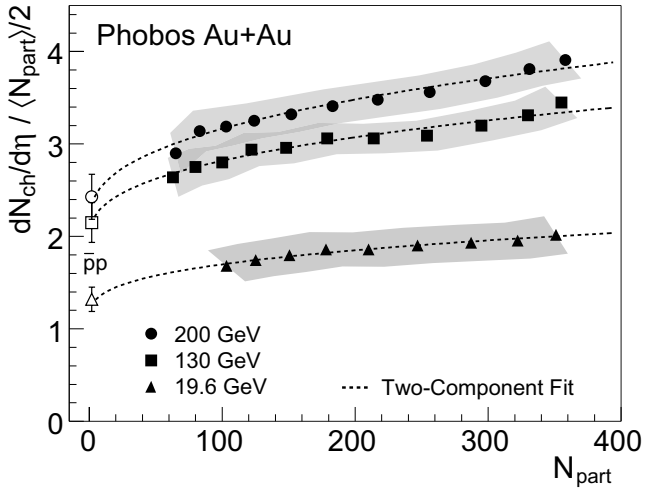

Fig. 4. Charged particles per participant pair as a function of number of participants in $\sqrt{s_{\rm NN}}$ = 19.6, 130 and 200 GeV Au+Au collisions measured by PHOBOS. The curves are two-component fits described in the text and in [16]

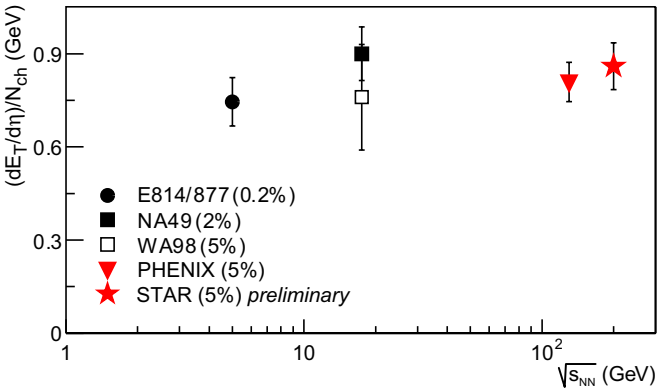

Fig. 5. $dE_T/d\eta|_{\eta=0}/dN_{ch}/d\eta|_{\eta=0}$ versus $\sqrt{s_{\rm NN}}$ for 5% most central events at AGS, SPS, and RHIC ([20,21])

produced from hard processes and one obtains values of 36% for $\sqrt{s_{\rm NN}}$ = 130 GeV, and 45% for 200 GeV, respectively [17]. A second class of calculations is based on parton saturation [18,19]; since the parton densities in the initial stage of the collision can be related to the density in the final state a parametrized dependence of the saturation scale Q_s on $\sqrt{s}$ and impact parameter allows one to predict $dN_{\rm ch}/d\eta$. However, the predictions from these and related models have been found to be almost indistinguishable when applied to RHIC data, especially because of the large experimental uncertainties in the calculation of $N_{\rm part}$ for very peripheral collisions, the region where the differences between the various models become more apparent. An exception are models based on final state saturation who significantly overpredict the yield at low $N_{\rm part}$. The systematic uncertainties in $N_{\rm part}$ for peripheral events can only be reduced when data from collisions of light ions, A< 100, become available.

Another important observable for characterizing the global properties of bulk matter is the transverse energy E_T. This was studied in detail by the PHENIX collaboration for $\sqrt{s_{\rm NN}}$ = 130 and PHENIX and STAR for 200 GeV [20,21] in the mid-rapidity region. They find that $dE_T/d\eta$ and $dN_{\rm ch}/d\eta$ increase with $N_{\rm part}$ in a very similar fashion resulting in an almost constant ratio $\langle E_T\rangle/\langle N_{\rm ch}\rangle \sim 0.9$ GeV. This holds for $\sqrt{s_{\rm NN}}$ = 130 *and* 200 GeV. Even more surprising is the fact that studies from Au+Au collisions at $\sqrt{s_{\rm NN}}$ = 4.8 and Pb+Pb collisions at 17.2 GeV yield very similar values, suggesting that the increased energy put into the system results solely in an increased particle production leaving the average energy per particle almost constant (see Fig. 5).

Bjorken studied boost invariant hydrodynamics [22] and derived a useful pocket formula for the energy density achieved in the central region:

$$\epsilon_{\rm Bj} = \frac{1}{\pi {R_A}^2 \tau} \frac{dE_T}{dy}, \quad (1)$$

where E_T is the transverse energy, R_A is the nuclear radius, and τ is the formation time, typically taken as ~ 1 fm/c, after which the hydrodynamic description is valid. From the measured $dE_T/d\eta$ for the 2% most central Au+Au collisions at 200 GeV PHENIX estimated the Bjorken energy density to be $\epsilon_{\rm Bj} \approx 5.5$ GeV/fm^3, assuming a conservative formation time of $\tau = 1$ fm/c. Similar studies at SPS in Pb+Pb collisions at $\sqrt{s_{\rm NN}} = 17.2$ GeV give $\epsilon_{\rm Bj} \approx 3.2$ GeV/fm^3 [23]. These values represent of course only a lower limit for the initial energy density since the longitudinal expansion of the system reduces the transverse energy considerably. Recent lattice results on QCD thermodynamics estimate the critical energy density to be $\epsilon \approx 0.70 \pm 0.35$ GeV/fm^3 [24], a value significantly surpassed already at SPS.

3.2 Thermodynamical behavior

One of the most important issues in the physics of heavy ion collisions is the question if, and if so at what stage, the produced system thermalizes and to what extent a thermal description is appropriate for the evolving system. The use of thermodynamic concepts to describe multi-particle production has a long history beginning with Hagedorn in the early 1960's [25]. The concept of a *temperature* applies, strictly speaking, only to systems in at least local thermal equilibrium. The measured hadron spectra contain two pieces of information: *(i)* their yields and ratios providing the chemical composition of the fireball at the chemical freeze-out point and *(ii)* their transverse momentum spectra that provide information about thermalization of the momentum distributions and collective flow. It is obvious that the observed single particle spectra do not reflect earlier conditions, *i.e.* the hot and dense deconfined phase, where chemical and thermal equilibrium may have been established, since rescattering erases most traces from the dense phase. Only those effects which are accumulative during the expansion, such as flow, remain.

As argued above, the relative population of the stable hadrons is fixed at chemical freezeout. Equilibrium at that point should be evident in the measured population ratios.The assumption of a locally thermalized source in chemical equilibrium can be tested by using statistical thermal models to describe the ratios of various emitted particles. This yields a baryon chemical potential μ_B, a strangeness saturation factor γ_s, and the temperature $T_{\rm ch}$ at chemical freeze-out. Because of the absence of any dynamic assumptions many details can never be fully absorbed by these models. Discrepancies between model and data up to 30% should be considered inside the systematic uncertainty of the thermal model approach [26]. So far these models are remarkably successful in describing

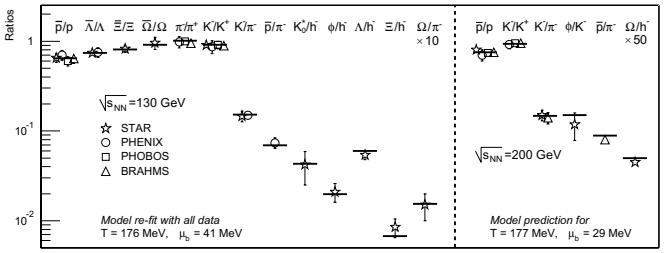

Fig. 6. Left panel: comparison between RHIC experimental particle ratios for $\sqrt{s_{\rm NN}} = 130$ GeV and statistical model calculations with $T_{\rm ch} = 176$ MeV and $\mu_B = 41$ MeV (from [29]). Right panel: comparison between RHIC ratios at $\sqrt{s_{\rm NN}} = 200$ GeV and prediction discussed in [29]

particle ratios at SPS [27,28] and now also at RHIC [29, 30]. This observation, together with the large collective flow (radial and elliptic) measured at RHIC, is generally considered a strong hint that chemical equilibrium is indeed reached. The wide reaching implications of thermal statistical models and the models themselves are still the subject of intense debate.

While the net-baryon chemical potential at chemical freeze-out is essentially determined by the baryon to antibaryon ratios ($\overline{p}/p, \overline{\Lambda}/\Lambda$ etc.), the non-identical particle ratios are the "thermometer" of the thermal statistical models. Figure 6 shows the comparison of measured particle ratios with *(i)* a statistical model fit for 130 GeV and *(ii)* model-related predictions for 200 GeV Au+Au collisions [29]. The predictions match well with the current results and indicate no significant change in $T_{\rm ch}$ but a drop in μ_B from ~ 41 MeV at $\sqrt{s_{\rm NN}} = 130$ GeV to 29 MeV at 200 GeV. The chemical freeze-out temperature is naturally limited by the confinement phase-transition temperature assumed to be around 175 MeV, although $T_{\rm ch}$ is actually not constrained in thermal model fits.

Transverse momentum spectra of identified particles reflect the system at kinetic freeze-out and allow us to extract information from the latest stage of the evolution when the system was still thermally coupled and governed by elastic interactions among its constituents. The measured inverse slope parameter is determined by two components: the actual temperature at the freeze-out and the transverse flow component, *i.e.*, collective radial expansion of the system. A thermalized system without any flow would yield plain exponential spectra in transverse mass $m_T = ({p_T}^2 + m^2)^{1/2}$, while the flow component results in a bowed shape; the higher the mass the more bowed the spectra.

The average inverse slope T of the spectra can, in simple terms, be approximated as $T = T_{\rm fo} + m\langle\beta_T\rangle^2$ where β_T is the transverse flow velocity and $T_{\rm fo}$ the temperature of the system at kinetic freeze-out. This ansatz, however, has the disadvantage that attempts to extract $T_{\rm fo}$ and β_T are strongly dependent on the range in which the slopes were determined. Of even greater concern is the assumption of a fixed flow velocity which oversimplifies the problem considerably. To overcome these problems full hydrodynamical model calculation are necessary that, at RHIC

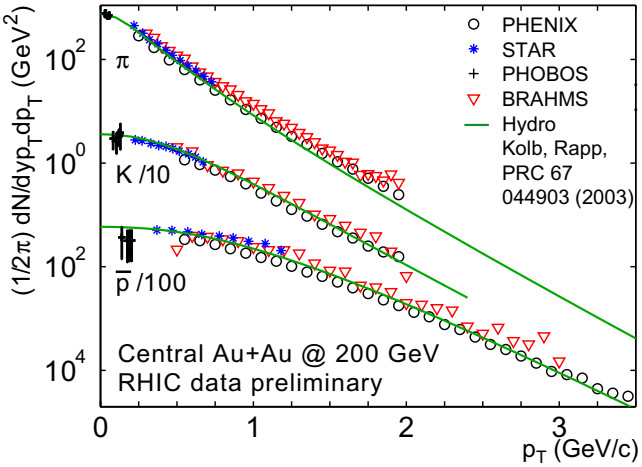

Fig. 7. Compilation of preliminary transverse momentum spectra of π^-, K^-, and $\overline{p}$ for 200 GeV central Au+Au collisions from all RHIC experiments. The curves are calculation from a hydrodynamical model calculation [33]

energies, describe the observed spectra very well [33] (see Fig. 7). To overcome the complexity of adjusting the initial energy density and the equation of state in a full hydrodynamical model calculation, many studies now use the so-called 'blastwave' parametrization [34]. The parametrization contains the essential hydrodynamic features but allows to extract flow velocity and freeze-out temperature by a simple fit to the spectra. Results are similar to those obtained from hydrodynamic models. While the so obtained freeze-out parameters at CERN/SPS energies yield $T_{\rm fo} = 122 - 127$ MeV and $\langle\beta_T\rangle = 0.48 \pm 0.01$ [32], fits to RHIC data give a slightly smaller freeze-out temperature $T_{\rm fo} \sim 110$ MeV but a higher flow value $\langle\beta_T\rangle = 0.55 - 0.6$ due to the higher pressure in the system [31].

3.3 Summary of soft physics

I cannot hope to address here all the soft physics observables that have been studied at RHIC. To conclude this section I will summarize a few of the main results, more detailed discussions can be found in ([13,15]).

- Low net-baryon density: antibaryon/baryon ratios at midrapidity are ∼0.6-1.0. The system is close to net-baryon free, similar to the early universe, but not precisely so. Finite baryon number is transported $\Delta y \sim 5.5$ rapidity units from the beam.
- There are strong indications that hadronic chemical equilibrium has been achieved at a temperature $T_{\rm ch}$ near the lattice critical temperature T_C.
- Hydrodynamic calculations describe well the transverse momentum spectra and collective flow.. The mass dependence of these observables, which is a sensitive test of the hydrodynamic picture, is described in detail.
- The energy density achieved early in the collision is estimated to be ~ 5.5 GeV/fm^3, exceeding the critical energy density derived from lattice QCD calculations by more than a factor of 5.
- Identical two-particle correlations (Hanbury Brown-Twiss correlations) are sensitive to the space-time evolution of the source. The extracted source radii and duration of freezeout show no significant increase relative to lower energy nuclear collisions. Such correlations measure only a piece of a dynamically expanding source and these results may indicate a very explosive expansion resulting from high early pressure.

4 Hard scattering at RHIC

The increase in $\sqrt{s_{\rm NN}}$ for nuclear collisions at RHIC relative to fixed target experiments opens up new channels to probe the dense medium generated in the collision. Jets with $E_T \sim 40$ GeV and higher are produced in sufficient numbers to provide robust observables. The measurement of jets in nuclear collisions poses a special problem, however: while the presence of a hard scattering in a nuclear collision can be detected (though in a biased way) via high p_T leading hadrons, the huge soft multiplicities contaminate any finite jet cone, spoiling the jet energy measurement. At sufficiently high E_T this effect may be minor (e.g. nuclear collisions at the LHC), but for the jet E_T currently accessible at RHIC it is fatal. We therefore restrict our considerations to leading particles and their correlations. We show below that hadrons with $p_T > 4$ GeV/c are produced dominantly from jet fragmentation, even in the most central Au+Au collisions.

Twenty years ago Bjorken [35] proposed that hard scattered partons in nuclear collisions could provide a sensitive probe of the surrounding medium. The energy loss $\mathrm{d}E/\mathrm{d}x$ due to elastic scattering of the partons in a Quark Gluon Plasma depends on the temperature as $T^2_{\rm plasma}$ and results in a suppression of the observed rate of jets or their leading hadrons at fixed p_T. Later work showed that $\mathrm{d}E/\mathrm{d}x$ from elastic scattering is negligible but that radiative energy loss in dense matter could be considerable [36, 37,38]. The energy loss is directly sensitive to the gluon density of the medium, $\rho_{\rm glue}$. While not a direct signature of deconfinement, measurement of $\rho_{\rm glue}$ that is substantially larger than in cold nuclear matter [39] is incompatible with the presence of a hadronic medium, thus large energy loss serves as an indirect signature of deconfinement.

There are currently several sets of measurements which address the question of partonic energy loss in dense matter, of which two I will discuss in turn: suppression of inclusive spectra and correlations of high-p_T hadron pairs.

4.1 High-p_T: Suppression of inclusive spectra

In p+p collisions at RHIC energies, hadrons with $p_T \sim 4$ GeV/c typically carry 75% of the energy of their parent jet, leading to the possibility that partonic energy loss in Au+Au collisions is reflected in the suppression of leading hadrons [38]. Hadron suppression is measured via the

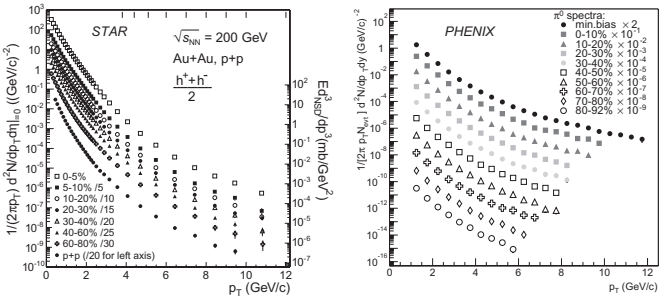

Fig. 8. Inclusive charged hadron invariant distributions from STAR (*left*) and for neutral pions from PHENIX (*right*) for various event centralities [40,41]

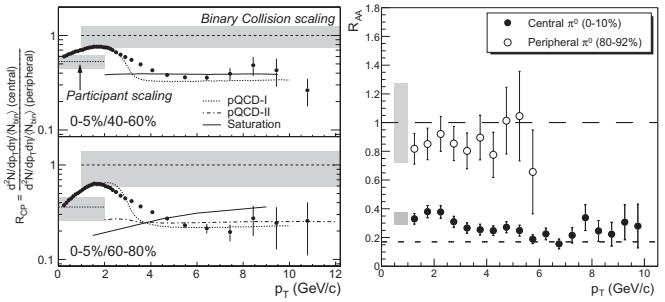

Fig. 9. Nuclear modification factor for Au+Au at $\sqrt{s_{\rm NN}}$= 200 GeV. Left: $R_{CP}(p_T)$for charged hadrons for two peripheral centrality bins. Error bars include both statistical and systematic uncertainties [40]. Right: $R_{AA}(p_T)$ for π^0 in central and peripheral collisions. The error bars include all point-to-point experimental errors [41]. In both plots the *shaded bands* represent uncertainties in the normalization that can move all points up or down together

nuclear modification factor:

$$R_{AA}(p_T) = \frac{d\sigma_{\rm AA}/dydp_T{}^2}{\langle N_{\rm bin}\rangle d\sigma_{\rm pp}/dydp_T{}^2} \qquad (2)$$

where $\sigma_{\rm pp}/dyd^2p_T$ is the inclusive cross section measured in elementary nucleon-nucleon collisions and $\langle N_{\rm bin}\rangle$ accounts for the geometric scaling from the elementary to nuclear collision. $R_{AA}(p_T)$ is normalized to be unity if Au+Au collisions are an incoherent superposition of p+p collisions. In addition to partonic energy loss, $R_{AA}(p_T)$ may be altered by nuclear effects such as gluon shadowing, which will reduce $R_{AA}(p_T)$, and the Cronin effect (multiple soft scattering in the initial state), which will increase it. These effects must be disentangled using measurements in simpler systems (in particular p+Au). Similar to $R_{AA}(p_T)$ is $R_{CP}(p_T)$ which describes the $\langle N_{\rm bin}\rangle$-normalized ratio of central and peripheral Au+Au spectra. The practical advantage of $R_{CP}(p_T)$ is that it extends to higher p_T than $R_{AA}(p_T)$, with significantly smaller uncertainties.

First indication of a strong suppression of high-p_T hadrons in nuclear collisions was reported from the 130 GeV data by both PHENIX and STAR [42]. The 200 GeV data have much higher statistics and both collaborations have now pushed this study well into the perturbative regime. Figure 8 shows on the left the inclusive charged hadron spectra as a function of centrality for p+p and Au+Au collisions at 200 GeV as measured by STAR [40], extending to p_T= 12 GeV. Shown on the right is the π^0 spectra from PHENIX [41]. Figure 9 shows $R_{CP}(p_T)$ and $R_{AA}(p_T)$ for these data. Suppression factors of 4-5 are observed in central collisions for both π^0s and charged hadrons, with weak, if any, dependence on p_T above $p_T \sim$ 5GeV/c. At asymptotically high jet E_T the relative energy loss should be negligible and $R_{AA}(p_T)$ and $R_{CP}(p_T)$ should return to unity. No evidence of this limiting high energy behavior is seen.

$R_{CP}(p_T)$ for $p_T < 6$ GeV/c is similar to measurements at $\sqrt{s_{\rm NN}}$ =130 GeV [42], but is now seen to be approximately constant for $5 < p_T < 12$ GeV/c. While different suppression factors have been reported for meson and baryon production in central Au+Au collisions for $2 < p_T < 4$ GeV/c [43], recent measurements indicate that all hadron species attain a similar suppression at the onset of the constant suppression region observed here [44]. It is consistent with $\langle N_{\rm part}\rangle$ scaling at $p_T \sim 4$ GeV/c as reported in [45], but is significantly below $\langle N_{\rm part}\rangle$ scaling at higher p_T.

The p_T-dependence of the suppression in Fig. 9 is well reproduced for $p_T > 5$ GeV/c by various perturbative QCD calculations [46,47]. All pQCD models incorporate nuclear shadowing of initial-state parton densities, the Cronin effect [48], and partonic energy loss containing energy loss. Other popular models such as the saturation picture [49] fails for the most peripheral bin. The magnitude of suppression is fit to the central collision data in the pQCD models but is predicted in the saturation calculation. Attenuation of initial jet formation due to multiple nucleon interactions [50] generates an increase in partonic $R_{AA}(p_T)$ for central collisions of a factor ~ 2 in $5 < E_T < 12$ GeV. Though the model does not incorporate fragmentation, a similar p_T-dependence would be expected for high-p_T hadrons, in contrast to observations. Suppression in the final state due to in-medium scattering of fragmentation hadrons also results in a rising $R_{AA}(p_T)$ with increasing p_T due to the dependence of hadron formation time on the total jet energy [51], though detailed comparison of this model to data requires further theoretical development.

4.2 High-p_T: Two-particle correlations

While jet fragmentation is reasonably expected to dominate hadron production at sufficiently high-p_T, it remains an open question whether the current measurements have achieved that limit. A full jet reconstruction in Au+Au events is not possible due to the complex underlying event, but intra-jet correlations amongst high-p_T hadrons are still visible and one can use these to map the transition in p_T from soft to hard physics. The rate of back-to-back di-jets may be especially sensitive to partonic energy loss effects: if one escapes from the surface, its partner has enhanced probability to plow through the bulk matter.

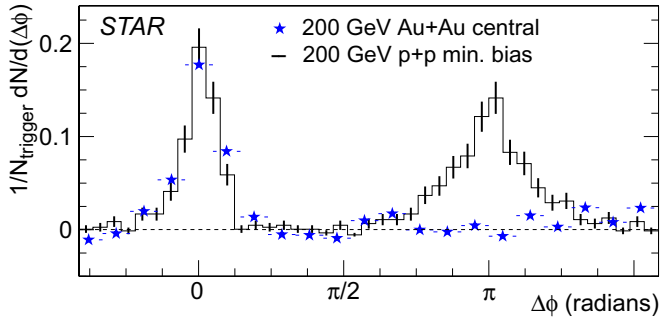

Fig. 10. Background subtracted azimuthal correlations of high-p_T hadron pairs in Au+Au compared to p+p [52]

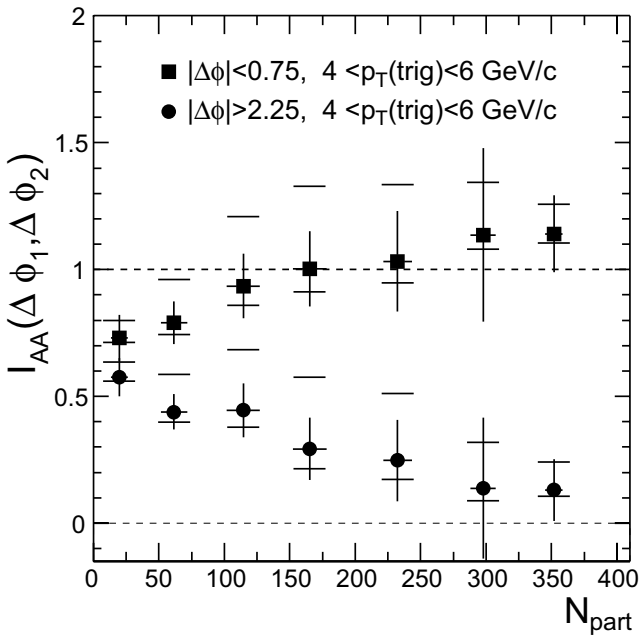

Fig. 11. I_{AA} vs centrality (*large* $N_{\rm part}$*=central collisions*) for near-angle (*upper*) and back-to-back (*lower*) angular correlations [52]. *Left:* trigger $p_T > 4$ GeV/c. *Right:* trigger $p_T > 3$ GeV/c

High-p_T hadron pairs with large azimuthal angle difference (back-to-back pairs) are the ideal tool to search for the effect of partonic energy loss on the di-jet (di-hadron) production rate [52]. Figure 10 shows the background subtracted azimuthal angular distribution between pairs for the most central Au+Au collisions at 200 GeV and, as a reference, for p+p collisions at the same energy. The background contribution of elliptic flow, *i.e.*, the azimuthal anisotropy in the particle emission in non-central events, and other non-jet effects are accounted for by means described in [52]. At all centralities, the near-angle peak is similar to the one observed in p+p, as is the large angle peak for peripheral collisions. Thus, back-to-back hadron pair production in peripheral nuclear collisions is well described by an incoherent superposition of 'background' sources (elliptic flow) and jet-like correlations measured in p+p. However, the large angle peak in the most central collisions is absent as depicted in Fig. 10. We are therefore led to a striking observation: back-to-back jet production is strongly suppressed in the most central Au+Au collisions.

The full centrality dependence of this effect can be quantified by plotting I_{AA}, the ratio of the integrated correlation peaks in Au+Au over those in pp, as a function of event centrality. Figure 11 shows I_{AA} as a function of $N_{\rm part}$ for trigger particles with $4 < p_T < 6$ GeV/c. The near-angle peak strength ($|\Delta\phi| < 0.75$) is near or above unity for all centralities and both thresholds: there is no suppression in the near-angle correlation. In contrast, the back-to-back correlation strength ($|\Delta\phi| > 2.25$) in Au+Au relative to p+p decreases smoothly from peripheral to central collisions. For the most central collisions the strength is consistent with zero, which would correspond to a complete suppression of the away-side hadron correlation rate above the threshold.

Various nuclear effects may contribute to the features seen in Fig. 11. Initial state multiple scattering might generate both the increase of the near-angle and suppression of the back-to-back correlation strength for more central collisions. The suppression in the most peripheral bin for Au+Au relative to p+p for both the near-angle and back-to-back peaks could be due to nuclear shadowing, or possibly the interplay between multiple scattering and absorption in matter. These issues will be clarified once the analysis of the data from the d+Au run at RHIC is completed.

4.3 Summary of high-p_T physics

This section reveals the following facts about high-p_T hadron production in Au+Au collisions at RHIC energies:

- Inclusive hadron production is suppressed in central collisions by a factor 4-5, with no strong p_T dependence within $5 < p_T < 12$ GeV/c.
- Near-angle two particle correlations show clear jet-like correlations for $p_T > 4$ GeV/c.
- Back-to-back two particle correlations show a striking suppression in central collisions.

All of these phenomena suggest a picture in which the system generated in nuclear collisions at RHIC is largely opaque to high energy partons and only those jets produced on the periphery of the reaction zone and heading outwards survive and are observed. This scenario naturally generates the suppression of the inclusive spectra as well as the strong suppression of back-to-back pairs. However, this picture as presented is only qualitative, and it remains to be shown whether a surface emission model can simultaneously describe all observed phenomena.

5 Conclusions and outlook

RHIC has had three successful data-taking periods. It has met its design luminosity goal for Au+Au, and has operated as the world's first polarized proton collider. The

runs in 2003 allow the study of asymmetric (d+Au) collisions for the first time in a collider. A long Au+Au run at top energy will occur in 2004, possibly with an energy scan at lower integrated luminosity.

An extensive array of measurements in the soft physics sector indicate the production of an equilibrated system at high temperature and pressure which blows apart rapidly. In the high-p_T sector, striking signals have been observed that suggest strong partonic energy loss resulting from a system at high energy density at early time, though there remain important puzzles and open questions.

I have not discussed the study of heavy quark production, which is in its infancy at RHIC. Charmonium suppression, a promising signature of deconfinement [9]. PHENIX has measured the inclusive electron spectrum, due primarily to charm [53], and recently reported the first measurement of J/Ψ at RHIC [54]. This physics will be a main focus of future runs.

References

1. J.C. Collins and M.J. Perry: Phys. Rev. Lett. **34**, 1353 (1975)
2. See for example K. Rajagopal these proceedings
3. K. Rajagopal and F. Wilczek: hep-ph/0011333
4. K. Kanaya: hep-ph/0209116
5. F. Karsch: Nucl. Phys. A **698**, 199c (2002)
6. Z. Fodor: hep-lat/0209191
7. D. Boyanovsky: hep-ph/0102120
8. N.K. Glendenning and F. Weber: astro-ph/0003426
9. J.W. Harris and B. Müller: Annu. Rev. Nucl. Part. Sci. B **46**, 71 (1966)
10. T. Roser: Nucl. Phys. A **698**, 23c (2002)
11. The Relativistic Heavy Ion Collider and Experiments: Nucl. Inst. Meth. A **499**, Issues 2-3 (2003)
12. Proceedings of Quark Matter 2001, Nucl. Phys. A **698**, (2002)
13. Proceedings of Quark Matter 2002: Nucl. Phys. A **715** (2003)
14. B.B. Back et al.: nucl-ex/0210015
15. T.S. Ullrich: Nucl. Phys. A **715**, 399c (2003)
16. D. Kharzeev and M. Nardi: Phys. Lett. B **507**, 121 (2001)
17. B.B. Back et al.: Phys. Rev. C **65**, 061901 (2002)
18. K.J. Eskola, K. Kajantie, and K. Tuominen: Phys. Lett. B **497**, 29 (2001)
19. D. Kharzeev and E. Levin: Phys. Lett. B **523**, 79 (2001)
20. A. Bazilevski: Nucl. Phys. A **715**, 486c (2003)
21. STAR collaboration: private communication
22. J.D. Bjorken: Phys. Rev. D **27**, 140 (1983)
23. T. Alber et al.: Phys. Rev. Lett. **75**, 3814 (1995)
24. F. Karsch: Nucl. Phys. A **698**, 199 (2002)
25. R. Hagedorn: Suppl. A. Nuovo Cimento Vol III, No.2 150 (1965)
26. U. Heinz: Nucl. Phys. A **661**, 140 (1999)
27. P. Braun-Munzinger, I. Heppe, and J. Stachel: Phys. Lett. B **465**, 15 (1999)
28. F. Becattini et al.: Phys. Rev. C **64**, 024901 (2001)
29. P. Braun-Munzinger et al.: Phys. Lett. B **518**, 41-46 (2001)
30. F. Becattini: J. Phys. G **28**, 1553 (2002)
31. G. Van Buren et al.: Nucl. Phys. A **715**, 129c (2003)
32. M. van Leeuwen et al.: Nucl. Phys. A **715**, 161c (2003)
33. P.F. Kolb and R. Rapp: Phys. Rev. C **67**, 044903 (2003)
34. E. Schnedermann, J. Sollfrank, and U. Heinz: Phys. Rev. C **48**, 2462 (1993)
35. J.D. Bjorken: FERMILAB-Pub-82/59-THY
36. M. Gyulassy and M. Plümer: Phys. Lett. B **432**, 121 (1990); R. Baier et al.: Phys. Lett. B **345**, 277 (1995)
37. R. Baier, D. Schiff, and B.G. Zakharov: Annu. Rev. Nucl. Part. Sci. B **50**, 37 (2000)
38. X.N. Wang and M. Gyulassy: Phys. Rev. Lett. **68**, 1480 (1992); X.N. Wang: Phys. Rev. C **58**, 2321 (1998)
39. E. Wang and X.N. Wang: Phys. Rev. Lett. **89**, 162301 (2002); F. Arleo: Phys. Lett. B **532**, 231 (2002)
40. J. Adams et al.: nucl-ex/0305015
41. S.S. Adler et al.: nucl-ex/0304022
42. K. Adcox et al.: Phys. Rev. Lett. **88**, 022301 (2002); C. Adler et al.: Phys. Rev. Lett. **89**, 202301 (2002)
43. J. Velkovska: Proceedings of Strange Quark Matter 2003, J. Phys. G. to be published
44. P. Sorenson et al.: nucl-ex/0305008
45. B.B. Back et al.: nucl-ex/0302015
46. X.N. Wang: nucl-th/0305010; private communication. Calculations use model parameters $\mu_0 = 2.0$ GeV and $\epsilon_0 = 2.04$ GeV/fm
47. I. Vitev and M. Gyulassy: Phys. Rev. Lett. **89**, 252301 (2002)
48. D. Antreasyan et al.: Phys. Rev. D **19**, 764 (1979); P.B. Straub et al.: Phys. Rev. Lett. **68**, 452 (1992)
49. D. Kharzeev, E. Levin, and L. McLerran: Phys. Lett. B **561**, 93 (2003); D. Kharzeev: private communication
50. R. Lietava, J. Pisut, N. Pisutova, and B. Tomasik: Eur. Phys. J. C **28**, 119 (2003)
51. K. Gallmeister, C. Greiner, and Z. Xu: Phys. Rev. C **67**, 044905 (2003)
52. C. Adler et al.: Phys. Rev. Lett. **90**, 082302 (2003)
53. K. Adcox et al.: Phys. Rev. Lett. **88**, 192302 (2002)
54. J. Nagle et al.: nucl-ex/0209015